

Controllable Phase Transition for Layered β -FeSe Superconductor Synthesized by Solution Chemistry

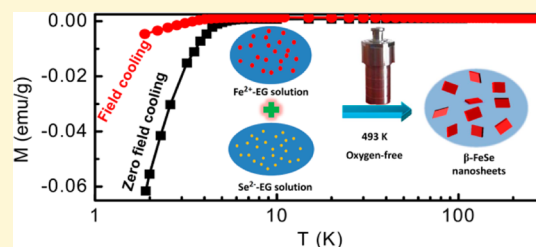
Da Li,^{*} Desheng Pan, Weilai Liu, Xiaoxi Li, Maolin Chen, Shaojie Li, Yong Li, Jun Tan, Dongming Sun, Zhenhua Wang,[†] Zheng Han, and Zhidong Zhang

Shenyang National Laboratory for Materials Science, Institute of Metal Research (IMR), Chinese Academy of Sciences (CAS), 72 Wenhua Road, Shenyang 110016, China

School of Material Science and Engineering, University of Science and Technology of China, Anhui 230026, China

S Supporting Information

ABSTRACT: Low-temperature synthesis of β -FeSe superconductor from soluble precursors is a great challenge in the chemical solution approaches. Here, we develop a new and facile solution-based synthetic route to first fabricate narrow-phased β -FeSe superconductor with soluble iron and selenium sources as starting materials. The growth mechanism of β -FeSe superconductors is discussed by kinetically controllable syntheses in various reaction conditions. Chemically engineering the stoichiometry of β -FeSe products by selenium-diffusion process gives rise to a transition of antiferromagnetic-superconducting-antiferromagnetic (AFM-SC-AFM) order. Once the AFM order is suppressed, SC β -FeSe nanosheets show a tunable initial superconducting transition temperature (T_C) from 3.2 to 10 K in the superconducting regime. Electrical measurements on superconducting β -FeSe exhibit an upper critical magnetic field higher than 14 T, showing potential application of β -FeSe nanosheet for superconducting device. This method provides guidance for future applications in such chemical solutions for diffusion-controlled synthesis of narrow-phased functional materials, which are enriched of abundant fundamental physics and potentials for future applications.



INTRODUCTION

Iron selenides, as an important family of inorganic functional materials, have attracted considerable interest in the synthesis and characterization owing to their outstanding physical properties and wide applications.^{1–4} In the binary iron–selenium system, NiAs-type FeSe (P63/mmc) is a magnetic semiconductor for spin-electronics application,⁵ while tetragonal phase β -FeSe with PbO structure is intriguing for superconductivity.⁶ Among the high-temperature iron-based superconductors, β -FeSe has the simplest layered crystal structure within the $P4/nmm$ space group,^{7,8} whose superconductivity properties have been subtle and can be tuned by engineering its composition and crystalline structure.^{9,10} Composition/structure-dependent physical behavior for the β -FeSe superconducting system attracted great attention not only due to its high T_C , but also for understanding the origin of iron-based superconductivity.¹¹

Several strategies have been employed for the synthesis of PbO-type β -FeSe and related solid solutions of Fe(Se,Te)¹² and Fe(S,Te).¹³ Conventional solid-state synthesis, such as solid-state reaction,⁶ flux method,¹⁴ and vapor self-transport route,¹⁵ require high temperatures above 700 °C and a long preparation period. Moreover, NiAs-type FeSe with ferrimagnetism often coexists and contaminates the superconducting β -FeSe in the products of the solid-state synthesis.⁶ Chemical methods such as metal organic chemical vapor deposition and electrochemical deposition have been applied to grow β -FeSe

thin films^{16–18} and nanorod arrays.¹⁹ Superconducting β -FeSe nanocables,¹⁵ nanorods,¹⁹ nanoislands,²⁰ and ultrathin films with several unit cells thickness on SrTiO₃ substrate²¹ provided possibilities for the fundamental understanding of reduced dimensionality on the enhanced T_C .

Low-temperature chemical solution is another major route to fabricate iron chalcogenides that could avoid the formation of impurity phase of NiAs-type FeSe and offer the control of the morphology of the products featuring as nanosheets.^{22–27} However, so far, superconductivity has been missing in all PbO-type β -FeSe and related Fe(Se,Te) solid solutions synthesized with chemical-solution method using soluble selenium and iron sources as starting materials.^{22–28} It was claimed that the soluble precursors of Fe and Se are incompatible for producing superconducting β -FeSe; instead, insoluble powders of iron and selenium are mandatory.²⁹ As is known, the superconductivity of β -FeSe within a narrow phase regime is highly sensitive to its stoichiometry.^{6,30} Therefore, the precise control of stoichiometric ratio between soluble iron and selenium in the reaction system may be the key factor for having superconducting β -FeSe, which has been overlooked thus far.

Here, we show a new facile solvothermal route with precise control of the molar ratio between Fe and Se in the chemical

Received: November 16, 2016

Revised: December 13, 2016

Published: December 14, 2016

solution system, which gives rise to phases of β -FeSe nanosheets with controllable transition of antiferromagnetic-superconducting-antiferromagnetic (AFM-SC-AFM) order. By optimizing a fixed amount of iron and selenium precursors as the starting materials, we are able to fine-tune the stoichiometry of β -FeSe by adjusting the contents of sodium hydroxide (NaOH, a selenium-buffer) in the solutions. This synthetic method allows selective syntheses of iron selenides from FeSe₂ to Fe₃Se₄, and to β -FeSe. By controlling the diffusion of Se atoms, β -FeSe nanosheets were fabricated in solution, showing controllable transition of AFM-SC-AFM order, with a tunable T_C from 3.2 to 10 K in the SC regime. This method provides guidance for future applications in such chemical solutions for diffusion-controlled synthesis of narrow-phased functional materials.

■ EXPERIMENTAL SECTION

Materials. The iron selenides nanostructures were synthesized by using commercially available reagents. Selenium powder (Se, 99.999%), iron(II) sulfate heptahydrate (FeSO₄·7H₂O, 99.0%–101%), sodium hydroxide (NaOH, 96.0%), polyvinylpyrrolidone (PVP, K30), hexadecyl trimethylammonium bromide (CTAB), sodium dodecyl sulfate, sodium salt (SDS), ethanol (99.7%), and ethylene glycol (EG, 99.0%) were purchased from Sinopharm Chemical Reagent Co. Ltd. (Shenyang, China). All chemicals were used as received without any further purification.

Synthesis of FeSe₂, Fe₃Se₄, and β -FeSe with Se Powders. A mixture of Se powder (1 mmol, 78.9 mg), FeSO₄·7H₂O (0.75 mmol, 208.5 mg), PVP (50 mg), and NaOH was dissolved under magnetic stirring in EG (20 mL) for 0.5 h. In a nitrogen atmosphere, the mixture was sealed into a Teflon-lined stainless steel autoclave (50 mL) and then maintained at 493 K for 24 h for the solvothermal reaction. After being cooled to room temperature, the resulting samples were washed with 10 mL of ethanol five times to remove the surfactants and solvents. Finally, the precipitate was dried in vacuo at room temperature and store in a glovebox with an argon atmosphere (the partial pressure of O₂ lower than 2 ppm) for further characterization. If the mixture was sealed with air in a Teflon-lined stainless steel autoclave, the products would always contain a small amount of impurity (Fe₃O₄). The phase components in the products are strongly dependent on the amount of NaOH changed from 10 to 520 mg in the reaction system. In a typical synthesis of single phase FeSe₂, the additive NaOH is 10 mg, while more than 360 mg of NaOH could form single phase β -FeSe. The mixture of Se powder (1.46 mmol, 115.3 mg), FeSO₄·7H₂O (0.75 mmol, 208.5 mg), PVP (50 mg), and NaOH (5 mmol, 200 mg) was dissolved in EG (20 mL) for the synthesis of single phase Fe₃Se₄.

Synthesis of β -FeSe with Se-Containing Solution. The solvothermal synthesis may be affected by varying the form of Se precursor.²² In a typical synthesis procedure of β -FeSe, a mixture of Se powder (1 mmol, 78.9 mg), PVP (60 mg), NaOH (11 mmol, 440 mg), and EG (10 mL) was first sealed in a Teflon-lined stainless steel autoclave (50 mL) and then maintained at 453 K for 3 h to obtain the black Se-containing solution. FeSO₄·7H₂O (0.75 mmol, 208.5 mg) was dissolved in 10 mL of EG to obtain the FeSO₄·7H₂O-EG solution. At room temperature, the FeSO₄·7H₂O-EG solution was added into the Se-containing solution under vigorous magnetic stirring. In a nitrogen atmosphere, the mixed solution was tightly sealed in a Teflon-lined stainless steel autoclave, which would be heated to 433 K and kept at this temperature for 12 h and then maintained at 493 K for 24 h.

Influence of Surfactant and Reaction Time on the Synthesis of β -FeSe. Besides the presence of polymer surfactant PVP, the roles of cationic surfactant CTAB and anionic surfactant SDS were explored in the solvothermal syntheses with different reaction time. In a typical synthesis procedure of β -FeSe, a mixture of Se powder (0.5 mmol, 39.5 mg), PVP (50 mg), CTAB (5 mg), NaOH (5.5 mmol, 220 mg), and EG (10 mL) was sealed in a Teflon-lined stainless steel autoclave (50 mL) and then maintained at 453 K for 3 h to obtain the Se-

containing solution. After the FeSO₄·7H₂O (0.375 mmol, 104.3 mg)-EG solution was mixed with the Se-containing solution under vigorous magnetic stirring, the mixed solution was tightly sealed in a Teflon-lined stainless steel autoclave in a nitrogen atmosphere, which was heated to 433 K and kept at this temperature for 12 h and then maintained at 493 K for a reaction time of 24, 48, 72, and 96 h, respectively.

The solvothermal synthesis of iron selenides was optimized by varying the amount of NaOH, the Fe:Se molar ratio, the form of Se precursor, the surfactant, or the reaction time, as summarized in Table S1 (Supporting Information).

Characterization. The X-ray diffraction (XRD) patterns of the iron selenides were collected by a Rigaku D/Max-2400 diffractometer equipped with a Cu K α radiation source ($\lambda = 0.154056$ nm) in the 2θ range of 10–85° with a step size of 0.02°. The size and morphology of the iron selenides were observed by using a JSM 6301F field-emission scanning electron microscope (SEM) system. Element compositions of the iron selenides were analyzed by Oxford energy dispersive X-ray (EDX) spectroscopy. Transmission electron microscopy (TEM), high-resolution TEM (HRTEM), and selected area electron diffraction (SAED) were taken on FEI Tecnai G2 F20 microscope operated at an acceleration voltage of 200 kV. The samples were prepared by evaporating a drop of dilute solution of β -FeSe nanosheets dispersed in absolute ethanol on an amorphous carbon-copper grid.

Temperature-dependent magnetic susceptibility in the field-cooling (FC) and zero-field-cooling (ZFC) modes (1.9–300 K, $H = 10$ –100 Oe) and isothermal magnetization (-30 kOe $\leq H \leq 30$ kOe) were measured on the as-prepared samples with a Quantum Design MPMS (XL-7) SQUID magnetometer. Hysteresis loops for the as-prepared β -FeSe nanosheets after the FC process in 50 kOe down from 300 K also were measured by a vibrating sample magnetometer (VSM) standard option in the PPMS equipped with a superconducting magnet of a maximum magnetic field of 14 T in a temperature range between 2 and 100 K. The as-prepared powder samples were fixed into capsules by varnish to minimize diamagnetic contributions from the background and to protect from oxidation. Electrical resistivity was measured using the electrical transport option (ETO) in the PPMS by the ac four-probe method on a compacted β -FeSe pellet. The pellet was obtained by compacting the as-prepared β -FeSe nanosheets with a diameter of 10 mm using a 1.2 GPa axial pressure with a steel die. Electrical transport of an individual β -FeSe nanosheet was also measured by the ac four-probe method in the PPMS with a current of 200 nA at a zero field.

■ RESULTS AND DISCUSSION

The effects of NaOH on the synthesis of iron selenides in a high purity nitrogen atmosphere are presented in Figure 1. Figure 1a shows the powder XRD pattern of the as-prepared FeSe₂ obtained from the reaction precursor solution containing 10 mg NaOH. All the XRD peaks are in good agreement with the Joint Committee on Powder Diffraction Standards (JCPDS) XRD card (82–0269) for FeSe₂ without ambiguous reflections. FeSe₂ is in the orthorhombic crystal structure with the unit cell lattice parameters of $a = 0.48002$ nm, $b = 0.57823$ nm, and $c = 0.35834$ nm. With increasing the amount of NaOH, Fe₃Se₄ and β -FeSe appear (Figures 1b–e). Moreover, single phase β -FeSe (Figure 1f) and Fe₃Se₄ (Figure 1g) have been controllably synthesized by simply adjusting the contents of NaOH and Se powder in the precursor solutions. Continually adjusting the NaOH addition from 280 to 520 mg (not shown) produces single phase β -FeSe. Different from those obtained using other precursors, solvents, and surfactants,^{2,22,24,31} the present synthetic route not only allows selective synthesis of iron selenides, but also controls their unique morphologies by conveniently adjusting the concentration of NaOH in the reaction system. The analysis of FeSe₂ and Fe₃Se₄ nanostructures can be found in Figures S1 and S2.

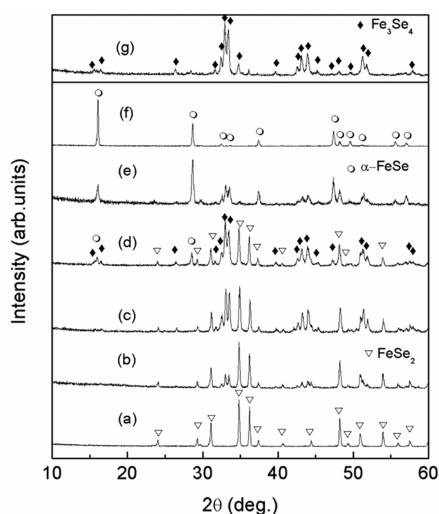


Figure 1. XRD patterns of the iron selenides synthesized with different NaOH content of (a) 10 mg, (b) 40 mg, (c) 80 mg, (d) 120 mg, (e) 200 mg, (f) 280 mg, and (g) 200 mg plus extra Se.

Besides the Fe_3Se_4 nanoflowers assembled from nanoplates to minimize the magnetostatic energy, the morphologies of FeSe_2 nanoprisms and $\beta\text{-FeSe}$ nanosheets may strongly relate to nucleation and growth of the crystals.³²

Further, we will focus on the discussion of the as-prepared $\beta\text{-FeSe}$. The values of T_C for the $\beta\text{-FeSe}$ samples synthesized with different NaOH addition (Figure 2) are close to 6 K, a bit lower

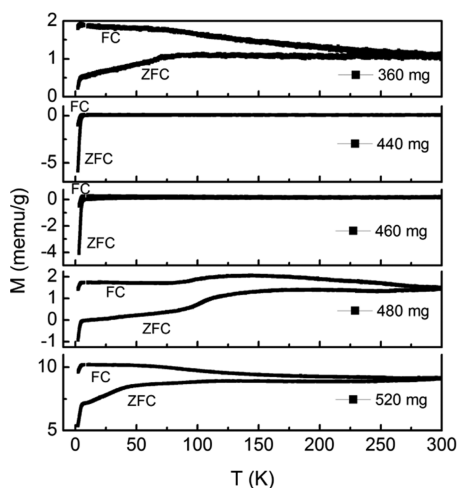


Figure 2. ZFC and FC magnetization curves (2–300 K) in a magnetic field of 10 Oe of the $\beta\text{-FeSe}$ samples obtained with various NaOH additions.

than that of bulk.⁶ Obviously, the superconducting volume fractions are dependent on the amount of NaOH, whose optimal addition is determined to be 440 mg. Figure 3a presents that all the powder XRD peaks of the sample synthesized with Se-containing solution can be indexed to the tetragonal $\beta\text{-FeSe}$, with calculated lattice constants of $a = 0.3776$ nm and $c = 0.5517$ nm. The lattice constant slightly expands in the a axis, but almost the same in the c axis as compared with the $\beta\text{-FeSe}$ (JCPDS XRD card 85–0735) ($a = 0.3765$ nm and $c = 0.5518$ nm). Tetragonal $\beta\text{-FeSe}$ has a layered crystal structure as shown in Figure 3b. Polymer surfactant PVP is easily absorbed on the (100) crystal face of $\beta\text{-FeSe}$

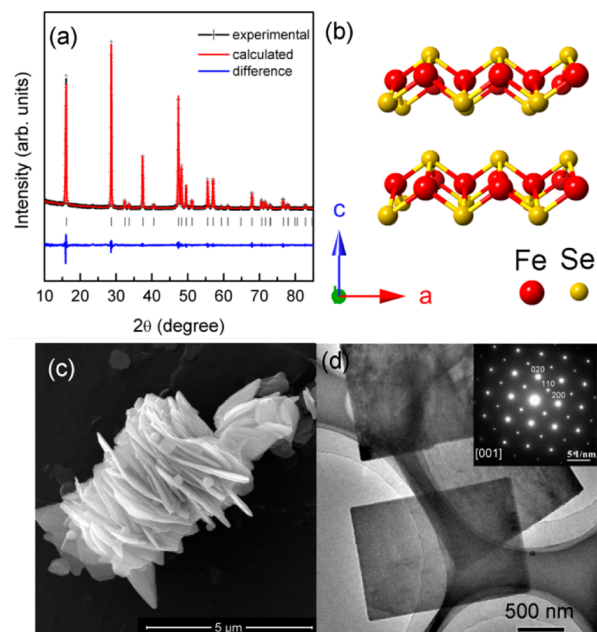


Figure 3. (a) XRD pattern of FeSe nanosheets (solid crosses) with Rietveld refinement and difference curve. The vertical bars indicate the Bragg reflection positions. (b) Crystal structure of $\beta\text{-FeSe}$. (c) SEM and (d) TEM images of $\beta\text{-FeSe}$ nanosheets. Inset: SAED pattern for a nanosheet.

FeSe and thereby reduces the growth rate along the [001] direction.²⁵ The two-dimensional (2D) quadrangle nanosheet morphology was confirmed by the SEM image (Figure 3c) and the TEM image (Figure 3d). The HRTEM image of a nanosheet (Figure S3) shows a lattice fringe spacing of 0.19 nm, which represents the (200) planes of the tetragonal $\beta\text{-FeSe}$. The selected area electron diffraction (SAED) pattern for a nanosheet viewed along the [001] direction (the inset of Figure 3d) is consistent with the $\beta\text{-FeSe}$, which indicates the single-crystalline nature of the individual nanosheet. The edge length of the $\beta\text{-FeSe}$ nanosheets varies from several hundreds of nanometers to above 10 μm and the thickness within 10–150 nm (Figure S4).

We now come to the effect of surfactant and reaction time on the $\beta\text{-FeSe}$ products. Entirely replacing PVP by cationic surfactant CTAB or SDS can also produce superconductivity in $\beta\text{-FeSe}$ with $T_C \approx 6$ K (Figure S5a,b). From the Meissner effect, the superconducting volume fraction of the $\beta\text{-FeSe}$ synthesized by CTAB is higher than that synthesized by SDS. By lowering the concentration of the precursors and using a mixed surfactants of PVP/CTAB in the synthesis, the $\beta\text{-FeSe}$ nanosheets with the reaction time of 24 h clearly presented magnetic anomaly at 125 K and incommensurate AFM order below 45 K (Figure S5c), while the nanosheets prepared with the mixed surfactant of PVP/SDS merely showed the incommensurate antiferromagnetism (Figure S5d).

Field-cooling (FC) hysteresis loops below 45 K show the exchange-bias behavior due to the exchange coupling between the weak-ferromagnetic and the antiferromagnetic components in these $\beta\text{-FeSe}$ nanosheets as shown in the inset of Figure S6. Both the coercivity (H_C) and the bias field (H_E) increase with lowering the temperature, which reach to 12.4 and 6.3 kOe at 2 K, respectively. With increasing the reaction time to 48 h, the $\beta\text{-FeSe}$ nanosheets synthesized with the surfactant of PVP/CTAB show a small amount of superconducting component with T_C

of 3.2 K (Figure S5e). By comparison, the β -FeSe nanosheets obtained from the surfactant of PVP/SDS show a ferromagnetic feature (Figure S5f). The PVP/SDS may be detrimental for the reaction of Fe^{2+} and Se^{2-} and preclude the formation of the β -FeSe superconductor.

To reveal the influence of selenium-diffusion mechanism on the syntheses of superconducting β -FeSe, more detailed experiments were performed with the excess selenium in the reaction system by extending reaction time (t) to prepare a series of β -FeSe samples. Figure S7 shows all the resultant samples in good agreement with the β -FeSe without impurity. Enlarged XRD patterns present shifts of diffraction peaks in a function of reaction time, for example, the shift of the (001) peaks shown in Figure 4a, where the arrows indicates the peak-

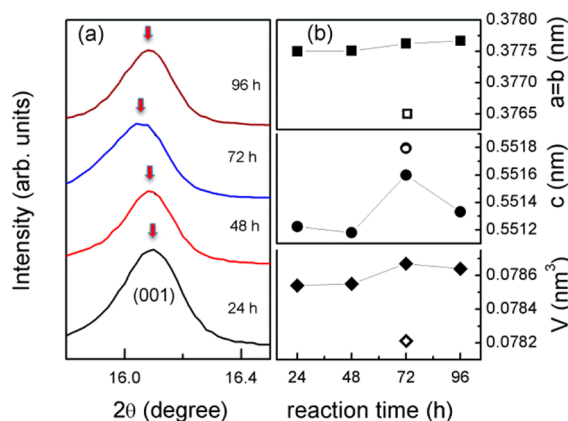


Figure 4. (a) Enlarged XRD patterns of the β -FeSe nanosheets synthesized at different reaction time. (b) Lattice constants (the solid symbols) versus the reaction time. The open symbols correspond to the β -FeSe (JCPDS XRD card 85–0735). The black lines in panel b are guides to the eye.

shift. The calculated lattice constants a , c and the cell volume V (Figure 4b) show an increase tendency with extending t from 24 to 72 h. The lattice constant c decreases at 96 h, which results in slight volume shrinkage. The β -FeSe nanosheets synthesized at 72 h have a close lattice constant c to that of β -FeSe (JCPDS XRD card 85–0735). The obvious increases in the lattice constant a and the cell volume V may be ascribed to the small size effect, while the shrink in the c axis may be due to the vacancies of Se in the iron-rich β -phases or Fe in the Se-rich β -phases. From SEM observations, unreacted Se nanospheres adhere on the β -FeSe nanosheets obtained at 24 h (Figure S8a). With increasing the reaction time from 48 to 96 h, the Se atoms diffuse into the nanosheets and the β -FeSe grew up in a layer-by-layer mode with a similar morphology (Figure S8b–d). Once the β -FeSe nucleates in the solution system, the initial nanosheets may serve as seeds and grow up by means of Ostwald ripening process.³³

Figure 5 presents the effect of the reaction time on the properties of these β -FeSe nanosheets. In Figure 5a, the β -FeSe nanosheets obtained at 24 h show a weak SC transition at about 3.2 K, but a distinct magnetic anomaly at $T_S = 125$ K and an AFM transition at $T_N = 45$ K. As the reaction time increases to 48 and 72 h (Figure 5b,c), the 125 K magnetic anomaly and the incommensurate AFM order have been strongly suppressed and the onset of T_C for β -FeSe superconductors gradually increases to about 6 and 10 K, respectively. The hysteresis loops of the β -FeSe superconductors in the insets of Figure 5b

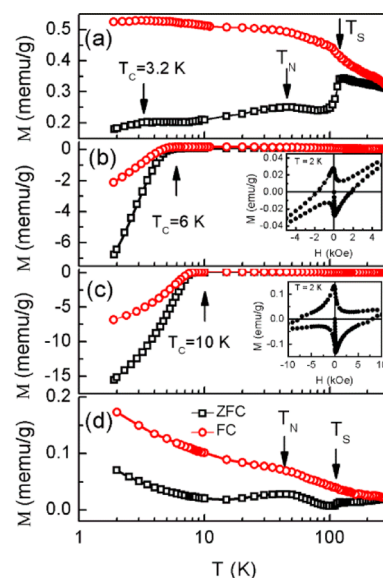
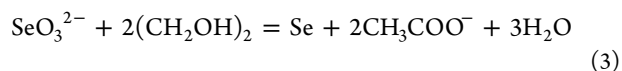


Figure 5. Field-cooling (FC) and zero-field-cooling (ZFC) magnetization versus temperature curves of the β -FeSe nanosheets synthesized with the reaction time of (a) 24 h, (b) 48 h, (c) 72 h, and (d) 96 h. Insets in panels b and c: M – H loops at 2 K.

and c show that the upper critical field of H_{C2} at 2 K increases from 1.8 kOe to 8.1 kOe. However, the Meissner effect lost with extending the reaction time to 96 h, while the 125 K magnetic anomaly and the incommensurate AFM order become pronounced again (Figure 5d). In an alkali medium system, Se disproportionates to SeO_3^{2-} and Se^{2-} anions, and then the Se^{2-} anions react with Fe^{2+} ions to produce β -FeSe, following the reaction formulas:



During the reaction process, the SeO_3^{2-} anions in the solution may be reduced by EG into element Se following the reaction eq 3, which disproportionates again to form SeO_3^{2-} and Se^{2-} anions in the present alkali solution system.²⁶ Sodium-hydroxide (NaOH) takes part in the reactions and serves as a selenium-buffer to precisely tune the stoichiometry of the β -FeSe samples, which present the transition of AFM-SC-AFM order.

The transition of AFM-SC-AFM order related to the reaction time should be ascribed to the evolution of stoichiometry in the β -samples. However, because of the error in the quantitative element analysis by the EDX, the precise evolution of Fe:Se molar ratio for the β -FeSe samples as a function of the reaction time was not determined here. In fact, bulk superconductivity was observed in the β - $\text{Fe}_{1.01}\text{Se}$ samples, while superconductivity was absent in the β - $\text{Fe}_{1.03}\text{Se}$ samples.³⁴ Iron-vacancy ordered β - $\text{Fe}_{0.80}\text{Se}$ (Se-rich) phase is antiferromagnetic, suggesting to the parent phase of the FeSe superconducting system.³⁵ However, the iron-rich region was the missing link in the temperature-doping phase diagram of Fe–Se system.³⁵ Our results confirm that both the iron-rich and the Se-rich β -FeSe phases are nonsuperconducting and antiferromagnetic below 45 K, whereas suitable Fe/Se stoichiometry can suppress the

antiferromagnetism of the chemically synthesized β -FeSe and reach superconductivity. On the basis of the observation in the chemically synthesized β -FeSe samples, a magnetic phase diagram for the FeSe superconducting system is proposed, as illustrated in Figure 6.

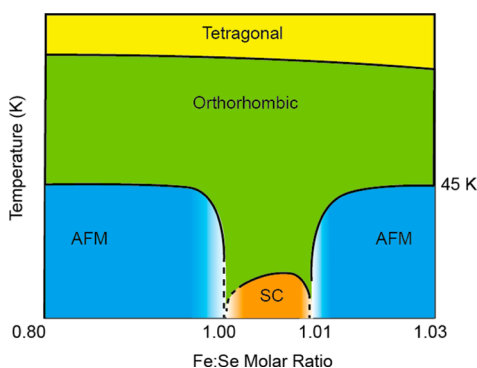


Figure 6. Sketch of the proposed temperature-doping phase diagram of Fe–Se superconducting system, showing the AFM and SC regions.

Temperature dependences of the resistivity (ρ) from 1.9 to 300 K measured on the as-synthesized β -FeSe compacted pellet and the same pellet but exposed under air atmosphere for 5 days (Figure 7) show the semiconducting-type conduction

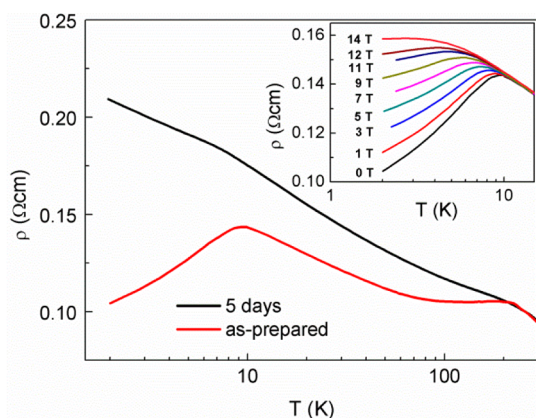


Figure 7. Temperature dependences of resistivity measured on (a) the as-synthesized β -FeSe pellet and (b) the same pellet but exposed under air atmosphere for 5 days. Inset: the resistivity versus temperature at different applied magnetic fields.

above 10 K. For the as-prepared β -FeSe pellet, the onset of the superconducting transition at about 10 K, corresponding to temperature where the resistivity begins to deviate from the normal state. However, the resistivity does not reach zero even the temperature dropping to 1.9 K. The resistivity versus temperature was recorded in the range of the superconducting transition under different applied magnetic fields (the inset of Figure 7). The resistivity increases gradually with the applied magnetic field and the onset of superconducting transition moves to lower temperatures. With the highest magnetic field up to 14 T, the superconducting transition is still observed, indicating that the upper critical magnetic field of the present β -FeSe pellet is higher than 14 T at 2 K. The increases of resistivity with the applied magnetic fields are obvious due to the magnetic fields destroying the superconducting state in the β -FeSe pellet.

It is noticed that the superconducting β -FeSe nanoparticles are unstable in air,²⁹ which degenerated to the antiferromagnetic phase. In our case, after exposed in air atmosphere for 5 days, the compacted β -FeSe pellet has lost superconductivity down to 1.9 K. Similarly, for an individual β -FeSe nanosquare, even though exposed in air for a very short amount of time during the device fabrication, the electrical transport shows no superconductivity down to 2 K (Figure 8). At higher

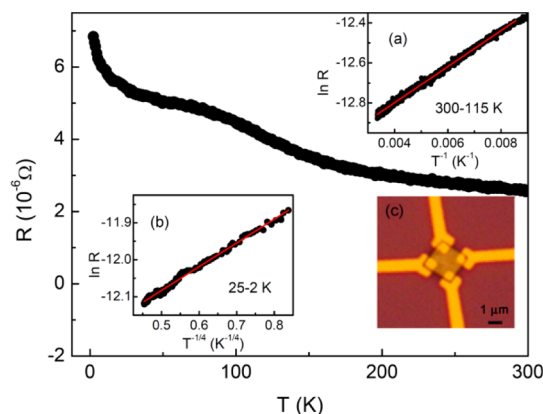


Figure 8. Temperature dependence of resistance (R) measured on an individual β -FeSe nanosheet. (a) Plot of $\ln R$ against T^{-1} between 115 and 300 K. (b) Plot of $\ln R$ against $T^{-1/4}$ between 2 and 25 K. (c) The optical photograph of the device for the electrical measurements.

temperatures ($T > 115$ K), the plot of $\ln(R) - T^{-1}$ in the inset of Figure 8a follows a linear relation, which indicates a typical semiconducting behavior. Below 115 K, there is an obvious transition in the RT curve possibly due to the magnetic anomaly. Over the temperature range from 25 to 2 K, the $R(T)$ curve presents a $T^{-1/4}$ -dependence (Figure 8b), which indicates the variable range hopping (VRH) conduction mechanism. Figure S9 shows the comparison of the as-synthesized superconducting β -FeSe nanosheets ($T_C \approx 6$ K) and those sealed with varnish and stored in a glovebox with the O_2 partial pressure lower than 2 ppm for around 70 days. The superconducting β -FeSe nanosheets with rigorous protection in an oxygen-free glovebox still exhibited the superconducting transition. It elucidates that an oxygen-free environment is critical to develop nanosized iron-based superconducting devices.

CONCLUSION

In summary, we present a new low-temperature chemical solution-based route to synthesize superconducting β -FeSe nanosheets with a capacity of mass production using nontoxic and inexpensive soluble selenium and iron sources as starting materials. Precise tuning the stoichiometry in β -FeSe by selenium diffusion mechanism gives rise to chemically synthesized β -FeSe phases with controllable transition of AFM-SC-AFM order. Chemical engineering the composition of β -FeSe superconductors reaches a tunable T_C from 3.2 to 10 K in the SC regime. The single crystal superconductive β -FeSe nanosheets have a high surface area, showing potential applications for future nanosized superconducting devices. Except for the requirement of oxygen-free condition, this newly developed low-temperature solvothermal route is facile to fabricate the iron-based superconductor by utilizing nontoxic and inexpensive soluble Fe and Se sources. Our method paves

the way, in chemical solutions, for diffusion-controlled synthesis of narrow-phased functional materials.

■ ASSOCIATED CONTENT

Supporting Information

The Supporting Information is available free of charge on the ACS Publications website at DOI: [10.1021/acs.chemmater.6b04887](https://doi.org/10.1021/acs.chemmater.6b04887).

Summary of iron selenides; SEM images and element analyses of FeSe₂ hexahedral prisms, Fe₃Se₄ nanoflowers, and β -FeSe sheet; hysteresis loops of Fe₃Se₄ nanoflowers; HRTEM image of β -FeSe nanosheet; TEM image of edge of several overlapped β -FeSe nanosheets; magnetization versus temperature in ZFC and FC models for β -FeSe samples; temperature dependence of coercivity and bias field for β -FeSe; XRD patterns of β -FeSe nanosheets; SEM images of β -FeSe nanosheets; ZFC and FC magnetization curves of β -FeSe nanosheets (PDF)

■ AUTHOR INFORMATION

Corresponding Author

*E-mail: dali@imr.ac.cn.

ORCID

Da Li: [0000-0001-9775-5650](https://orcid.org/0000-0001-9775-5650)

Zhenhua Wang: [0000-0003-4122-1873](https://orcid.org/0000-0003-4122-1873)

Author Contributions

The paper was written through contributions of all authors. All authors have given approval to the final version of the paper.

Notes

The authors declare no competing financial interest.

■ ACKNOWLEDGMENTS

The work is supported by the National Natural Science Foundation of China under Grant Nos. 51371175, 51331006, and 1150438.

■ REFERENCES

- (1) Wang, W. J.; Pan, X.; Liu, W. Q.; Zhang, B.; Chen, H. W.; Fang, X. Q.; Yao, J. X.; Dai, S. Y. FeSe₂ Films with Controllable Morphologies as Efficient Counter Electrodes for Dye-sensitized Solar Cells. *Chem. Commun.* **2014**, *50*, 2618–2620.
- (2) Fu, T. T.; Chen, Y. Y.; Hao, J. L.; Wang, X. Y.; Liu, G.; Li, Y. G.; Liu, Z.; Cheng, L. Facile Preparation of Uniform FeSe₂ Nanoparticles for PA/MR Dual-modal Imaging and Photothermal Cancer Therapy. *Nanoscale* **2015**, *7*, 20757–20768.
- (3) Wu, X. J.; Shen, D. Z.; Zhang, Z. Z.; Zhang, J. Y.; Liu, K. W.; Li, B. H.; Lu, Y. M.; Yao, B.; Zhao, D. X.; Li, B. S.; Shan, C. X.; Fan, X. W.; Liu, H. J.; Yang, C. L. On the Nature of the Carriers in Ferromagnetic FeSe. *Appl. Phys. Lett.* **2007**, *90*, 112105.
- (4) Thomas, E. L.; Wong-Ng, W.; Phelan, D.; Millican, J. N. Thermoprocess of Co-doped FeSe. *J. Appl. Phys.* **2009**, *105*, 073906.
- (5) Feng, Q. J.; Shen, D. Z.; Zhang, J. Y.; Li, B. S.; Li, B. H.; Lu, Y. M.; Fan, X. W.; Liang, H. W. Ferromagnetic FeSe: Structural, Electrical, and Magnetic Properties. *Appl. Phys. Lett.* **2006**, *88*, 012505.
- (6) Hsu, F. C.; Luo, J. Y.; Yeh, K. W.; Chen, T. K.; Huang, T. W.; Wu, P. M.; Lee, Y. C.; Huang, Y. L.; Chu, Y. Y.; Yan, D. C.; Wu, M. K. Superconductivity in the PbO-type Structure α -FeSe. *Proc. Natl. Acad. Sci. U. S. A.* **2008**, *105*, 14262–14264.
- (7) Margadonna, S.; Takabayashi, Y.; McDonald, M. T.; Kasperkiewicz, K.; Mizuguchi, Y.; Takano, Y.; Fitch, A. N.; Suard, E.; Prassides, K. Crystal Structure of the New FeSe_{1-x} Superconductor. *Chem. Commun.* **2008**, 5607–5609.

- (8) Takahashi, H.; Igawa, K.; Arii, K.; Kamihara, Y.; Hirano, M.; Hosono, H. Superconductivity at 43 K in an Iron-based Layered Compound LaO_{1-x}F_xFeAs. *Nature* **2008**, *453*, 376–378.

- (9) Mizuguchi, Y.; Tomioka, F.; Tsuda, S.; Yamaguchi, T.; Takano, Y. Superconductivity at 27 K in Tetragonal FeSe under High Pressure. *Appl. Phys. Lett.* **2008**, *93*, 152505.

- (10) Guo, J. G.; Jin, S. F.; Wang, G.; Wang, S. C.; Zhu, K. X.; Zhou, T. T.; He, M.; Chen, X. L. Superconductivity in the Iron Selenide K_xFe₂Se₂ (0 ≤ x ≤ 1.0). *Phys. Rev. B: Condens. Matter Mater. Phys.* **2010**, *82*, 180520.

- (11) Bohmer, A. E.; Arai, T.; Hardy, F.; Hattori, T.; Iye, T.; Wolf, T.; von Lohneysen, H.; Ishida, K.; Meingast, C. Origin of the Tetragonal-to-Orthorhombic Phase Transition in FeSe: A Combined Thermodynamic and NMR Study of Nematicity. *Phys. Rev. Lett.* **2015**, *114*, 027001.

- (12) Yeh, K. W.; Huang, T. W.; Huang, Y. L.; Chen, T. K.; Hsu, F. C.; Wu, P. M.; Lee, Y. C.; Chu, Y. Y.; Chen, C. L.; Luo, J. Y.; Yan, D. C.; Wu, M. K. Tellurium Substitution Effect on Superconductivity of the α -phase Iron Selenide. *Epl-Europhys. Lett.* **2008**, *84*, 37002.

- (13) Dong, C. H.; Wang, H. D.; Yang, J. H.; Qian, B.; Chen, J. A.; Li, Z. J.; Yuan, H. Q.; Fang, M. H. Effect of Annealing on Superconductivity in Fe_{1+y}(Te_{1-x}S_x) System. *Sci. China: Phys., Mech. Astron.* **2010**, *53*, 1216–1220.

- (14) Mok, B. H.; Rao, S. M.; Ling, M. C.; Wang, K. J.; Ke, C. T.; Wu, P. M.; Chen, C. L.; Hsu, F. C.; Huang, T. W.; Luo, J. Y.; Yan, D. C.; Ye, K. W.; Wu, T. B.; Chang, A. M.; Wu, M. K. Growth and Investigation of Crystals of the New Superconductor α -FeSe from KCl Solutions. *Cryst. Growth Des.* **2009**, *9*, 3260–3264.

- (15) Mishra, S.; Song, K.; Koza, J. A.; Nath, M. Synthesis of Superconducting Nanocables of FeSe Encapsulated in Carbonaceous Shell. *ACS Nano* **2013**, *7*, 1145–1154.

- (16) Li, L.; Yang, Z. R.; Sun, Y. P.; Zhang, J. Y.; Shen, D. Z.; Zhang, Y. H. Superconductivity and Magnetism in FeSe Thin Films Grown by Metal-organic Chemical Vapor Deposition. *Supercond. Sci. Technol.* **2011**, *24*, 015010.

- (17) Demura, S.; Ozaki, T.; Okazaki, H.; Mizuguchi, Y.; Kawasaki, Y.; Deguchi, K.; Watanabe, T.; Hara, H.; Yamaguchi, T.; Takeya, H.; Takano, Y. Electrochemical Synthesis of Iron-Based Superconductor FeSe Films. *J. Phys. Soc. Jpn.* **2012**, *81*, 043702.

- (18) Demura, S.; Tanaka, M.; Yamashita, A.; Denholme, S. J.; Okazaki, H.; Fujioka, M.; Yamaguchi, T.; Takeya, H.; Iida, K.; Holzapfel, B.; Sakata, H.; Takano, Y. Electrochemical Deposition of FeSe on RABiTS Tapes. *J. Phys. Soc. Jpn.* **2016**, *85*, 015001.

- (19) Zhou, S. M.; Lou, S. Y.; Wang, Y. Q.; Chen, X. L. Synthesis of Ordered α -FeSe Nanorod Array by CVD and its High T_C. *Mater. Lett.* **2011**, *65*, 1741–1743.

- (20) Mishra, S.; Song, K.; Ghosh, K. C.; Nath, M. Enhancement of Superconducting T_C (33 K) by Entrapment of FeSe in Carbon Coated Au-Pd_{1-x}Se₁₅ Nanoparticles. *ACS Nano* **2014**, *8*, 2077–2086.

- (21) Lee, J. J.; Schmitt, F. T.; Moore, R. G.; Johnston, S.; Cui, Y. T.; Li, W.; Yi, M.; Liu, Z. K.; Hashimoto, M.; Zhang, Y.; Lu, D. H.; Devereaux, T. P.; Lee, D. H.; Shen, Z. X. Interfacial Mode Coupling as the Origin of the Enhancement of T_C in FeSe Films on SrTiO₃. *Nature* **2014**, *515*, 245–U207.

- (22) Li, S. J.; Li, D.; Jiang, J. J.; Liu, G. B.; Ma, S.; Liu, W.; Zhang, Z. D. Growth Process and Magnetic Properties of α -FeSe Nanostructures. *J. Appl. Phys.* **2014**, *115*, 17B502.

- (23) Oyler, K. D.; Ke, X. L.; Sines, I. T.; Schiffer, P.; Schaak, R. E. Chemical Synthesis of Two-Dimensional Iron Chalcogenide Nanosheets: FeSe, FeTe, Fe(Se, Te), and FeTe₂. *Chem. Mater.* **2009**, *21*, 3655–3661.

- (24) Chen, L. Q.; Zhan, H. Q.; Yang, X. F.; Sun, Z. Y.; Zhang, J.; Xu, D.; Liang, C. L.; Wu, M. M.; Fang, J. Y. Composition and Size Tailored Synthesis of Iron Selenide Nanoflakes. *CrystEngComm* **2010**, *12*, 4386–4391.

- (25) Chen, L. Q.; Yang, X. F.; Fu, X. H.; Wang, C. M.; Liang, C. L.; Wu, M. M. Facile Solvothermal Synthesis of Uniform Iron Selenide Nanoplates. *Eur. J. Inorg. Chem.* **2011**, *2011*, 2098–2102.

- (26) Li, M. L.; Yao, Q. Z.; Zhou, G. T.; Fu, S. Q. Microwave-Assisted Synthesis of Flower-like β -FeSe Microstructures. *CrystEngComm* **2010**, *12*, 3138–3144.
- (27) Mao, X.; Kim, J. G.; Han, J. S.; Jung, H. S.; Lee, S. G.; Kotov, N. A.; Lee, J. Phase-Pure FeSe_x (x = 1, 2) Nanoparticles with One- and Two-Photon Luminescence. *J. Am. Chem. Soc.* **2014**, *136*, 7189–7192.
- (28) Pachmayr, U.; Fehn, N.; Johrendt, D. Structural transition and superconductivity in hydrothermally synthesized FeX (X = S, Se). *Chem. Commun.* **2016**, *52*, 194–197.
- (29) Greenfield, J. T.; Kamali, S.; Lee, K.; Kovnir, K. A Solution for Solution-Produced β -FeSe: Elucidating and Overcoming Factors that Prevent Superconductivity. *Chem. Mater.* **2015**, *27*, 588–596.
- (30) McQueen, T. M.; Huang, Q.; Ksenofontov, V.; Felser, C.; Xu, Q.; Zandbergen, H.; Hor, Y. S.; Allred, J.; Williams, A. J.; Qu, D.; Checkelsky, J.; Ong, N. P.; Cava, R. J. Extreme Sensitivity of Superconductivity to Stoichiometry in Fe_{1+ δ} Se. *Phys. Rev. B: Condens. Matter Mater. Phys.* **2009**, *79*, 014522.
- (31) Zhang, H.; Long, G.; Li, D.; Sabirianov, R.; Zeng, H. Fe₃Se₄ Nanostructures with Giant Coercivity Synthesized by Solution Chemistry. *Chem. Mater.* **2011**, *23*, 3769–3774.
- (32) Li, D.; Li, S. J.; Dong, B. J.; Yang, T.; Liu, W.; Zhang, Z. D. Large Magnetocrystalline Anisotropy of Fe_{3-x}Cr_xSe₄ Single Crystals due to Cr Substitution. *Epl-Europhys. Lett.* **2015**, *109*, 37004.
- (33) Hou, Y. L.; Kondoh, H.; Ohta, T. Self-assembly of Co Nanoplatelets into Spheres: Synthesis and Characterization. *Chem. Mater.* **2005**, *17*, 3994–3996.
- (34) McQueen, T. M.; Williams, A. J.; Stephens, P. W.; Tao, J.; Zhu, Y.; Ksenofontov, V.; Casper, F.; Felser, C.; Cava, R. J. Tetragonal-to-Orthorhombic Structural Phase Transition at 90 K in the Superconductor Fe_{1.01}Se. *Phys. Rev. Lett.* **2009**, *103*, 057002.
- (35) Chen, T. K.; Chang, C. C.; Chang, H. H.; Fang, A. H.; Wang, C. H.; Chao, W. H.; Tseng, C. M.; Lee, Y. C.; Wu, Y. R.; Wen, M. H.; Tang, H. Y.; Chen, F. R.; Wang, M. J.; Wu, M. K.; Van Dyck, D. Vacancy Order and Superconductivity in Tetragonal β -Fe_{1-x}Se. *Proc. Natl. Acad. Sci. U. S. A.* **2014**, *111*, 63–68.